INORGANIC CHEMISTRY
FRONTIERS

RESEARCH ARTICLE

View Article Online
View Journal | View Issue

Cite this: *Inorg. Chem. Front.*, 2023, **10**, 2107

Low temperature molten salt synthesis of noncentrosymmetric $(NH_4)_3SbF_3(NO_3)_3$ and centrosymmetric $(NH_4)_3SbF_4(NO_3)_2$†

Qin Wang,[a] Jinxuan Ren,[a] Dan Wang,[a] Liling Cao,[a] Xuehua Dong,[a] Ling Huang,*[a] Daojiang Gao[a] and Guohong Zou*[b]

Received 10th December 2022,
Accepted 28th February 2023

DOI: 10.1039/d2qi02637f

rsc.li/frontiers-inorganic

Two fluorine antimony nitrates named $(NH_4)_3SbF_3(NO_3)_3$ and $(NH_4)_3SbF_4(NO_3)_2$ have been successfully synthesized by a low temperature molten salt method. Although these two title compounds possess NO_3^- groups and similar Sb-polyhedra, they exhibit completely different macroscopic centricities, $(NH_4)_3SbF_3(NO_3)_3$ being noncentrosymmetric while $(NH_4)_3SbF_4(NO_3)_2$ being centrosymmetric, which is induced by the discrepant coordination environments of Sb^{3+}. Interestingly, the noncentrosymmetric $(NH_4)_3SbF_3(NO_3)_3$ exhibits a strong second harmonic generation response (3.3 × KDP), a large birefringence (0.098@546 nm) and a large band gap (3.77 eV), indicating its potential as a UV nonlinear optical material. Detailed structure–property analysis confirms that the superior optical property is due to the synergistic effect of the planar π-conjugated NO_3^- groups and the stereochemically active lone pair containing Sb^{3+} cations.

Introduction

At present, nonlinear optical (NLO) materials, which are the pivotal component of the solid-state laser, have developed to an important branch of modern optics and are widely used in information, medical, scientific research, military and industrial manufacturing fields.[1–6] In general, an ideal NLO crystal should meet the following conditions: large nonlinear optical coefficient, appropriate birefringence, wide transmission range, high laser damage threshold, stable physicochemical properties, and so on.[7–10] In fact, few compounds could satisfy all of the above conditions, for some of the criteria are contradictory. Therefore, the design and synthesis of NLO materials with excellent overall properties has become a great challenge.

It is well known that the primary characteristic of a NLO crystalline material is that it has a noncentrosymmetric (NCS) structure; that is, the compound must crystallize in a noncentrosymmetric space group.[11,12] It has been found that the reasonable combination of different asymmetric chromophores is an effective tactic for the synthesis of NLO materials, which is conducive to the generation of large second harmonic generation (SHG) response.[13,14] Common asymmetric chromophores include (1) planar π-conjugated anions, such as BO_3^{3-}, CO_3^{2-}, and NO_3^-;[15–17] (2) distorted polyhedra of d^0 and d^{10} transition metal ions, such as Ti^{4+}, Mo^{6+}, Zn^{2+}, and Hg^{2+};[18–22] (3) lone pair electron cations with stereochemical activity, such as Pb^{2+} and Bi^{3+}.[23–25] In comparison to planar π-conjugated anionic ions, the BO_3^{3-} system is relatively mature at present, and numerous splendid NLO crystals have been obtained, such as β-BaB_2O_4 (β-BBO),[26] LiB_3O_5 (LBO),[27] and $KBe_2BO_3F_2$ (KBBF).[28] The CO_3^{2-} anion is unstable and easily decomposed at high temperatures, and the crystal growth of carbonates is difficult. Moreover, among them, NO_3^- has been proved to be a splendid functional anion to constitute NLO materials because of its large microscopic second-order polarization and mild synthesis conditions conducive to the growth of large-sized single crystals.[29,30] As for the cationic ions, compounds containing metal ions (Pb^{2+}, Bi^{3+}, Sn^{2+}, and Sb^{3+}) with lone pair electrons always exhibit excellent NLO properties, such as $Pb_3Mg_3TeP_2O_{14}$ (13.5 × KDP),[31] $K_2Bi_2(SO_4)_2Cl_4$ (5.5 × KDP),[32] $[Sn_2(H_2PO_2)_3]Br$ (3.0 × KDP)[33] and $K_2Sb(P_2O_7)F$ (4.0 × KDP).[34] Among them, the development of antimony(III)-based nonlinear optical crystal materials is proceeding slowly due to the easy oxidation and hydrolysis of Sb^{3+}. In the mid- and far-infrared region, some Sb(III)-chalcogenides have been reported,[35,36] whereas in the ultraviolet region, few antimony(III)-based oxide or oxyfluoride nonlinear optical materials have been reported due to the difficulty in the crystal growth.

[a]*College of Chemistry and Materials Science, Sichuan Normal University, Chengdu, 610066, P. R. China*
[b]*College of Chemistry, Sichuan University, Chengdu, 610065, P. R. China.*
E-mail: huangl026@sina.com, zough@scu.edu.cn

†Electronic supplementary information (ESI) available: Additional crystallographic data, crystal photographs, XRD patterns, TGA curves, XRD patterns after melting, IR spectra and band structures calculation. CCDC 2222170 and 2222171. For ESI and crystallographic data in CIF or other electronic format see DOI: https://doi.org/10.1039/d2qi02637f

Compared with the aqueous phase reactions like hydrothermal and aqueous solution methods, molten salt synthesis could provide an anhydrous environment for the reaction, which would effectively solve the oxidation and hydrolysis problems. Conventional molten salts tend to have a high melting point, which is not suitable for the system containing Sb^{3+} cations; the exploration of a suitable molten salt is required.[37] Ionic liquids (ILs) are a novel type of low temperature molten salt; they show advantages in material synthesis in some specific fields.[38,39] However, they are organic salts composed of entirely ionic species, and the products of these reactions are extremely sensitive to air and moisture; a proper inorganic molten salt with a low melting point would be a better choice.[40] Nitrates possess the ability to dissolve many inorganic and organic compounds, for that nitrates exhibit low melting point temperature; especially, NH_4NO_3 has a melting point as low as 170 °C, and it could be used as a good medium for the reaction. In addition, molten salt nitrates can also provide NLO functional units in the reaction to construct NLO materials.

Based on the above views, SbF_3 with active lone pair electrons was combined with a low temperature molten salt nitrate NH_4NO_3 to explore novel NLO materials, and two ammonium antimony nitrates named $(NH_4)_3SbF_3(NO_3)_3$[41] and $(NH_4)_3SbF_4(NO_3)_2$ were successfully obtained. The two title compounds possess the same chemical composition but different atomic ratios, which induce their discrepant coordination modes of Sb^{3+} and opposite symmetries. In particular, the NCS compound $(NH_4)_3SbF_3(NO_3)_3$ reveals a large SHG efficiency of about 3.3 × KDP and large birefringence of 0.098@546 nm.

Experimental section

Synthesis of $(NH_4)_3SbF_3(NO_3)_3$ and $(NH_4)_3SbF_4(NO_3)_2$

The reaction reagents NH_4F (≥96.0%) and SbF_3 (≥99.8%) were purchased from Aladdin, and NH_4NO_3 (≥99.7%) was purchased from Xi Long Chemical without further purification.

Nitrate with a low melting point is a good reactant for the synthesis of molten salt method. We first mixed NH_4NO_3 and SbF_3 in a ratio of 3 : 1 for $(NH_4)_3SbF_3(NO_3)_3$ and 2 : 1 for $(NH_4)_3SbF_4(NO_3)_2$. Then, no further reagent was added for the synthesis of $(NH_4)_3SbF_3(NO_3)_3$, and 1 mmol NH_4F (0.037 g) was added for $(NH_4)_3SbF_4(NO_3)_2$. After the mixture was fully ground, it was placed in a Teflon autoclave and heated at 100 °C for 4 days. Then the mixture was cooled to room temperature at a rate of 5 °C h^{-1}. Colorless bulk crystals of $(NH_4)_3SbF_3(NO_3)_3$ and $(NH_4)_3SbF_4(NO_3)_2$ were obtained, respectively (Fig. S1†). Notably, the atomic ratio of the synthesized compounds is exactly the same as that of the raw materials. Therefore, the molten salt of nitrates could not only provide the anhydrous environment to inhibit the hydrolysis of Sb^{3+}, but also participate in the reaction as reactants. By adjusting the ratio of raw materials, the products change accordingly; hence, the molten salt method could make the synthesis of novel compounds more effective.

Table 1 Crystal data and structure refinement for $(NH_4)_3SbF_3(NO_3)_3$ and $(NH_4)_3SbF_4(NO_3)_2$

Formula	$(NH_4)_3SbF_3(NO_3)_3$	$(NH_4)_3SbF_4(NO_3)_2$
Formula weight	418.91	374.07
Crystal system	Monoclinic	Orthorhombic
Space group	$P2_1$	*Pnma*
a (Å)	9.0362(4)	12.6805(4)
b (Å)	7.4301(3)	12.3608(3)
c (Å)	9.5591(4)	7.0737(2)
α (°)	90	90
β (°)	101.118(4)	90
γ (°)	90	90
V (Å^3)	629.75(5)	1108.74(5)
Z	2	4
ρ(calcd) (g cm^{-3})	2.209	2.241
Temperature (K)	297.07(10)	295.94(10)
λ (Å)	0.71073	0.71073
F (000)	408.0	725.0
μ (mm^{-1})	2.284	2.535
R_1, wR_2 ($I > 2\sigma(I)$)[a]	0.0389/0.1046	0.0189/0.0401
R_1, wR_2 (all data)	0.0422/0.1082	0.0234/0.0415
GOF on F^2	1.042	1.067
Flack parameter	0.04(2)	—

[a] $R_1(F) = \sum||F_o| - |F_c||/\sum|F_o|$. w$R_2(F_o^2) = [\sum w(F_o^2 - F_c^2)^2/\sum w(F_o^2)^2]^{1/2}$.

Single crystal structure determination

The crystal structures of $(NH_4)_3SbF_3(NO_3)_3$ and $(NH_4)_3SbF_4(NO_3)_2$ were measured using a Rigaku XtaLAB Synergy R diffractometer, and determined by the direct method through SHELX-2014.[42] The coordinates of all the atoms were solved by the least square plane convergence algorithm based on F^2 full matrix. Finally, PLATON was used to check the space group, and there was no higher space group.[43] The crystallographic data and other relevant data of the two compounds are presented in Table 1 and Tables S1–S4.†

Powder X-ray Diffraction

A Smart Lab powder X-ray diffractometer with Cu-Kα radiation was adopted to measure the powder X-ray diffraction spectrum of the target compounds, with a rate of 8° min^{-1}, a 2θ range of 5–70° and a scanning step width of 0.02°.

Thermal analysis

Thermogravimetric analysis (TGA) measurements were carried out on a Discovery-TGA thermal analyzer. The crystalline material was loaded into a platinum crucible and heated from 0 °C to 800 °C at 10 °C min^{-1} under a N_2 atmosphere.

Infrared spectroscopy

The infrared spectra of the two title compounds were measured using a Vertex 70 Fourier transform infrared spectrometer (FTIR) with KBr as the background. KBr (100 mg) and powder samples (1 mg) of the title compounds were thoroughly mixed in an agate mortar and then pressed into transparent plates with a diameter of 13 mm and a thickness

of about 1 mm. The wavelength range was 400 cm^{-1} to 4000 cm^{-1}.

UV–Vis diffuse reflectance spectroscopy

$(NH_4)_3SbF_3(NO_3)_3$ and $(NH_4)_3SbF_4(NO_3)_2$ were tested using a Shimadzu UV-2600 spectrophotometer at room temperature with $BaSO_4$ as a standard reference, and the test range was 185–800 nm.

Birefringence measurements

The birefringence characteristics of $(NH_4)_3SbF_3(NO_3)_3$ and $(NH_4)_3SbF_4(NO_3)_2$ were measured using a polarizing microscope (Carl Zeiss Axioscope 5). The wavelength of the light source is 546 nm.

Frequency-doubling effect

The powder SHG signal of $(NH_4)_3SbF_3(NO_3)_3$ was measured by the Kurtz and Perry method under a Q-switched Nd:YAG laser with 1064 nm radiation.[44] $(NH_4)_3SbF_3(NO_3)_3$ samples were divided into six different sizes (25–45, 45–58, 58–75, 75–106, 106–150 and 150–212 μm) for testing, and the particle size of KH_2PO_4 (KDP) references was consistent with that of $(NH_4)_3SbF_3(NO_3)_3$ samples.

Theoretical calculations

In order to understand the electronic structures of the two compounds more clearly, their band structures, density of states (DOS) and partial density of states (PDOS) were calculated by density functional theory (DFT).[45] The Perdew–Burke–Ernzerhof (PAW-PBE) functional was used in the calculation,[46] as implemented in the Vienna *Ab initio* Simulation Package (VASP).[47–50] The *k*-points in the Brillouin band were set to be 4 × 7 × 4 for $(NH_4)_3SbF_3(NO_3)_3$ and 3 × 3 × 5 for $(NH_4)_3SbF_4(NO_3)_2$, respectively, and the cutoff kinetic energy was set to 550 eV for both of them.

Results and discussion

Crystal structure description

$(NH_4)_3SbF_3(NO_3)_3$ crystallizes in a NCS space group of $P2_1$, consisting of one Sb atom, three F atoms, three N atoms, nine O atoms, and three NH_4^+ cations. In this compound, each Sb atom forms the $[SbF_3]$ complex with three F atoms (Fig. 1a), and the distance between the Sb–F bond is 1.921–1.968 Å. The $[SbF_3]$ complex and the NO_3^- unit are arranged separately in the crystal. NH_4^+ is distributed in the cavity of the entire crystal as a charge compensation unit, which is represented by a grey tetrahedron. The $[SbF_3]$ complex and NO_3^- moiety are further linked with NH_4^+ through N–H···O and N–H···F hydrogen bonds, with the hydrogen bond length in the range of 2.033–2.159 Å and 1.892–2.614 Å, respectively (Fig. 1b).

$(NH_4)_3SbF_4(NO_3)_2$ crystallizes in a centrosymmetric (CS) space group of *Pnma*, consisting of one Sb atom, four F atoms, six O atoms, two N atoms and three NH_4^+. In $(NH_4)_3SbF_4(NO_3)_2$, the Sb atom forms the $[SbF_4]^-$ anion group with four F atoms (Fig. 1c), and the Sb–F bond distance is in the range of 1.941–2.073 Å. NO_3^- is independently arranged in the crystal with the N–O bond distance in the range of 1.240–1.247 Å. NH_4^+, as a charge balancing unit, connects the $[SbF_4]^-$ and NO_3^- units into a 3D network framework through N–H···F and N–H···O hydrogen bonds (Fig. 1d). The lengths of N–H···F and N–H···O hydrogen bonds are in the ranges of 1.843–2.060 Å and 2.028–2.171 Å, respectively.

It is generally accepted that the crystal structure of a compound is determined more by the basic structural unit than by

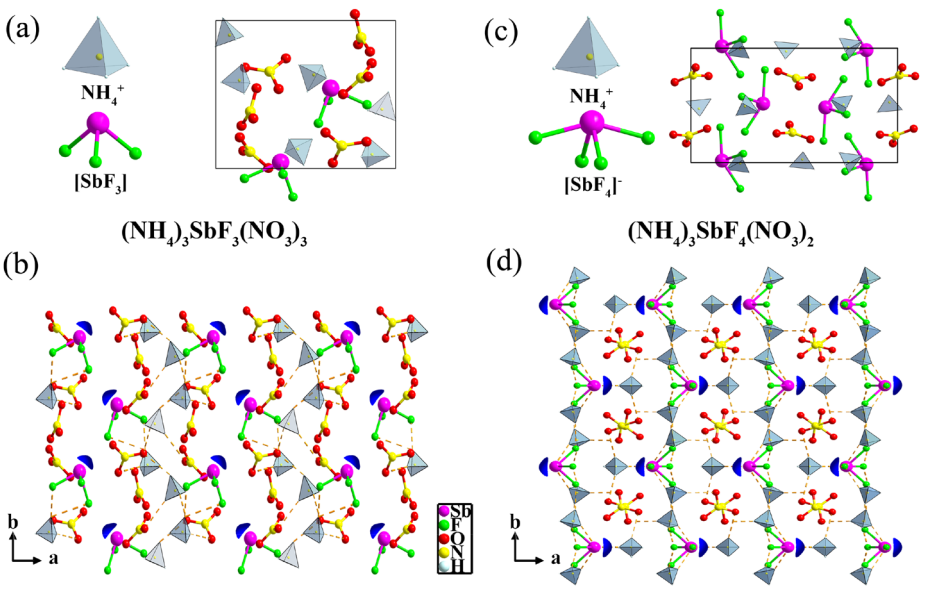

Fig. 1 (a and c) The representations of different coordination modes of Sb^{3+} and a unit cell. (b and d) The arrangement mode of $(NH_4)_3SbF_3(NO_3)_3$ and $(NH_4)_3SbF_4(NO_3)_2$.

the chemical composition. As can be seen from the above descriptions, although $(NH_4)_3SbF_3(NO_3)_3$ and $(NH_4)_3SbF_4(NO_3)_2$ possess the same chemical composition, the different atomic ratio induces the coordination discrepancy of Sb^{3+}. Therefore, the different basic building units with different degrees of distortion may ultimately lead to their structural discrepancy. NCS $(NH_4)_3SbF_3(NO_3)_3$ contains a tri-coordinated $[SbF_3]$ complex that is scattered, and the lone pair electrons of Sb^{3+} show two directions that are left and right symmetric along the *b* axis (Fig. 1b). Sb^{3+} with different directions are alternately aligned, and the compound $(NH_4)_3SbF_3(NO_3)_3$ exhibits a final NCS structure. In $(NH_4)_3SbF_4(NO_3)_2$, the Sb atom bridges four F atoms to form a twisted seesaw $[SbF_4]^-$ complex, and the lone pair electrons of Sb atoms also exhibit two orientations that are anti-parallel along the *a*-axis. NO_3^- in $(NH_4)_3SbF_4(NO_3)_2$ also has anti-parallel orientations along the *c* axis. For that anti-parallel arrangement of basic units usually leads to a centrosymmetric structure, and hence $(NH_4)_3SbF_4(NO_3)_2$ ultimately presents the CS structure as shown in Fig. 1d. Understanding the key factors dominating the symmetries of crystals and the structure–property relationship is helpful in the exploration of novel NLO materials.

Powder X-ray diffraction

Powder X-ray diffraction was carried out on $(NH_4)_3SbF_3(NO_3)_3$ and $(NH_4)_3SbF_4(NO_3)_2$, respectively. The phase purity of the two compounds was verified for that the experimental results were consistent with the fitting results of single crystal X-ray diffraction (Fig. S2†).

Thermal properties

Thermogravimetric analysis was performed for $(NH_4)_3SbF_3(NO_3)_3$ and $(NH_4)_3SbF_4(NO_3)_2$, respectively. As shown in Fig. S3,† $(NH_4)_3SbF_3(NO_3)_3$ could stabilize to 100 °C, while $(NH_4)_3SbF_4(NO_3)_2$ started to decompose at 220 °C. After heating from 100 °C to 800 °C under a nitrogen atmosphere, the total weight loss of the former is about 70%, while that of the latter is about 50%. X-ray powder diffraction was used to determine the heating products of the two compounds, and the final residue was confirmed to be Sb_2O_4 in both cases, as shown in Fig. S4.† $(NH_4)_3SbF_3(NO_3)_3$ and $(NH_4)_3SbF_4(NO_3)_2$ possess the same chemical composition, and the difference in their thermal stability may be caused by their different hydrogen bonds.[51] Compounds with higher hydrogen bond density and shorter hydrogen bond length always exhibit better thermal stability. Comparing the two title compounds, their hydrogen bond densities are 0.03335 and 0.03788 $Å^{-3}$, respectively, and the shortest hydrogen bond of 1.843 Å exists in $(NH_4)_3SbF_4(NO_3)_2$; therefore, $(NH_4)_3SbF_4(NO_3)_2$ should have better thermal stability, which is consistent with the experimental value.

Optical properties

The IR spectra for $(NH_4)_3SbF_3(NO_3)_3$ and $(NH_4)_3SbF_4(NO_3)_2$ have been measured and are shown in Fig. S5.† The strong bands around 3200 and 1400 cm^{-1} in $(NH_4)_3SbF_3(NO_3)_3$ and $(NH_4)_3SbF_4(NO_3)_2$ can be attributed to anti-symmetric stretching and bending of the N–H bond. The absorption peaks at 1338, 1042 cm^{-1} in $(NH_4)_3SbF_3(NO_3)_3$ and 1378, 1052 cm^{-1} in $(NH_4)_3SbF_4(NO_3)_2$ are mainly attributed to the symmetric/asymmetric stretching vibration of the NO_3^- group, and the medium peaks at 832/720 cm^{-1} and 837/737 cm^{-1} could be attributed to the bending vibrations of the NO_3^- group. The characteristic absorption peaks at 561/506/466 cm^{-1} and 556/518/452 cm^{-1} originate from the asymmetric stretching and bending vibrations of the Sb–F bond. All the assignments are consistent with previous reports.[52,53]

UV-Vis diffuse reflectance spectroscopy was performed on the compounds $(NH_4)_3SbF_3(NO_3)_3$ and $(NH_4)_3SbF_4(NO_3)_2$. It can be seen that their band gaps are 3.77 eV and 3.64 eV, with cutoff edges of 330 nm and 340 nm, respectively (Fig. 2a and b), indicating that the two title compounds are potential UV crystalline materials.

The birefringence of $(NH_4)_3SbF_3(NO_3)_3$ and $(NH_4)_3SbF_4(NO_3)_2$ was determined using a Carl Zeiss Axioscope 5 polarizing microscope (Fig. 2c). $(NH_4)_3SbF_3(NO_3)_3$ exhibits a moderate birefringence of 0.098@546 nm, while $(NH_4)_3SbF_4(NO_3)_2$ exhibits a large birefringence of 0.164@546 nm, indicating that both compounds are potential birefringent materials. As studied by Lin *et al.*, the introduction of highly polar anisotropic building units with ordered arrangement would induce large birefringence.[54] Comparing the orientations of lone pair electrons of Sb^{3+} and π-conjugated NO_3^- groups, in $(NH_4)_3SbF_3(NO_3)_3$, the lone pair electrons with two directions show a certain angle, and NO_3^- anions also represent a chaotic arrangement. However, in $(NH_4)_3SbF_4(NO_3)_2$, the lone pair electrons are completely parallel to the *a* axis; meanwhile, NO_3^- anions are parallel to the *c* axis. The parallel arrangement of polar functional units is conducive

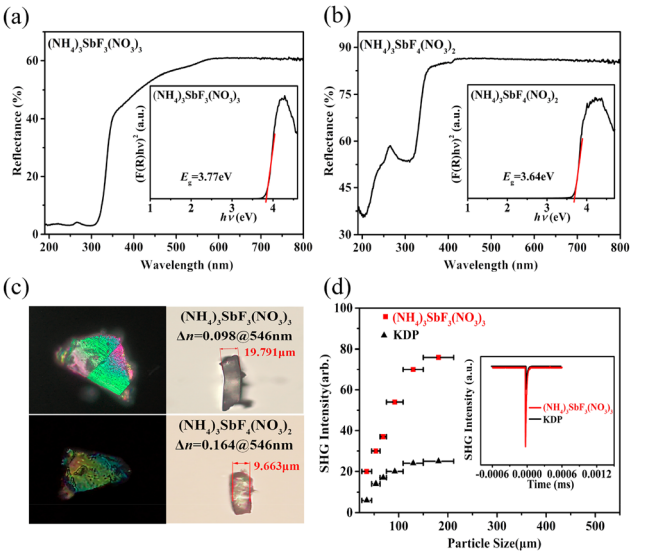

Fig. 2 (a and b) The UV optical diffuse reflectance spectra of $(NH_4)_3SbF_3(NO_3)_3$ and $(NH_4)_3SbF_4(NO_3)_2$. Inset: the Tauc plot of $(F(R)h\nu)^2$ *versus* $h\nu$ for the band-gap energy. (c) The birefringence measurement results of $(NH_4)_3SbF_3(NO_3)_3$ and $(NH_4)_3SbF_4(NO_3)_2$. (d) The phase-matching curve and SHG intensity for $(NH_4)_3SbF_3(NO_3)_3$ with KDP as the reference (150–212 μm).

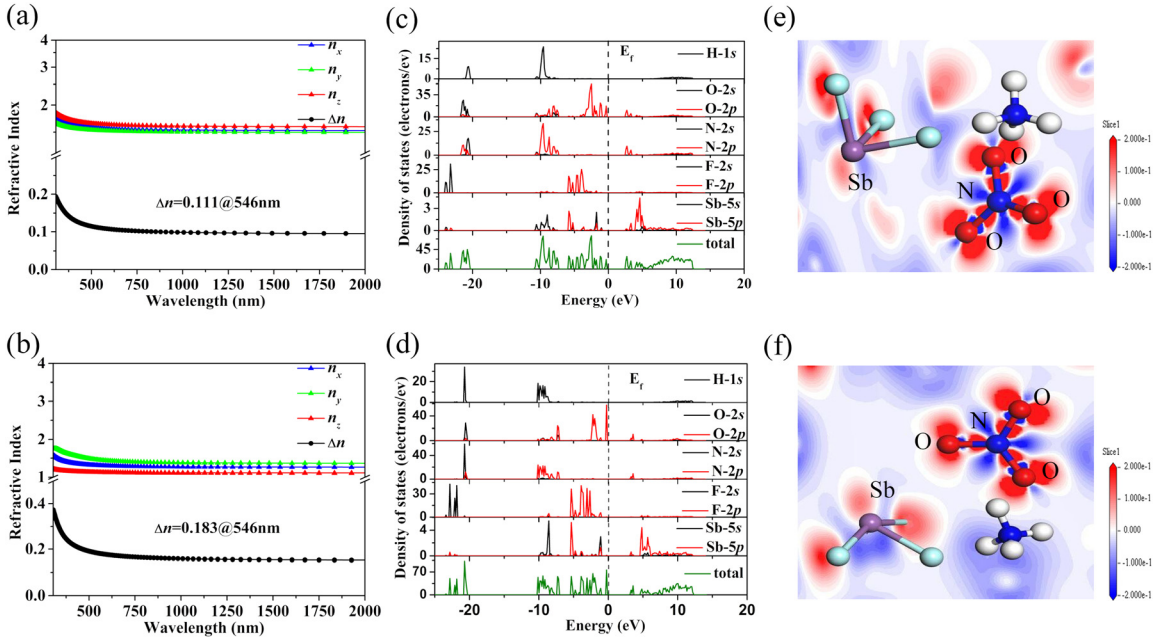

Fig. 3 (a and b) Calculated refractive indexes for compounds $(NH_4)_3SbF_3(NO_3)_3$ and $(NH_4)_3SbF_4(NO_3)_2$. (c and d) The total DOS and partial DOS of $(NH_4)_3SbF_3(NO_3)_3$ and $(NH_4)_3SbF_4(NO_3)_2$. The Fermi level is set to 0 eV. (e and f) Electron-density difference maps of $(NH_4)_3SbF_3(NO_3)_3$ and $(NH_4)_3SbF_4(NO_3)_2$.

to the generation of large birefringence; therefore, $(NH_4)_3SbF_4(NO_3)_2$ with a CS structure exhibits much larger birefringence than NCS $(NH_4)_3SbF_3(NO_3)_3$.

NLO properties

Since $(NH_4)_3SbF_3(NO_3)_3$ belongs to the NCS $P2_1$ space group, KH_2PO_4 (KDP) was used as the reference sample for the SHG test. As shown in Fig. 2d, with the increase of grain size of $(NH_4)_3SbF_3(NO_3)_3$, the SHG response increases first and tends to be constant gradually, indicating that $(NH_4)_3SbF_3(NO_3)_3$ is type I phase-matchable. Meanwhile, the SHG signal intensity map of $(NH_4)_3SbF_3(NO_3)_3$ shows a strong frequency doubling signal value of about 3.3 × KDP, which could be attributed to the lone pair electrons of Sb^{3+} and the high density of NO_3^- anions.

Theoretical calculations

The refractive index dispersion curves of $(NH_4)_3SbF_3(NO_3)_3$ and $(NH_4)_3SbF_4(NO_3)_2$ have been calculated, which show appropriate anisotropy (Fig. 3a and b). Taking $(NH_4)_3SbF_3(NO_3)_3$ as an example, $n_z > n_x > n_y$, where n_x, n_y and n_z represent the refractive index in the x, y and z directions, respectively. According to the formula $\Delta n = n_z - n_y$, the birefringence index Δn is calculated to be 0.111@546 nm for $(NH_4)_3SbF_3(NO_3)_3$ and 0.183@546 nm for $(NH_4)_3SbF_4(NO_3)_2$, which are in good agreement with the experimental values.

In order to explore the intrinsic relationship between the structure and optical properties for the two title compounds, systematic theoretical calculations were performed based on density functional theory. The direct band gaps of $(NH_4)_3SbF_3(NO_3)_3$ and $(NH_4)_3SbF_4(NO_3)_2$ calculated by PBE were 2.95 eV and 3.20 eV, respectively (Fig. S6†), which were 0.82 eV and 0.44 eV lower than the experimental values.[55] The total and partial state densities (TDOS/PDOS) were also calculated for the two title compounds (Fig. 3c and d), which are similar in terms of structural similarity. The results show that in the range of −25 to 0 eV, the valence bands of these two compounds are mainly from H-1s, O-2p, N-2p, and F-2p orbitals, with a small amount from Sb-5p and O-2s orbitals. From 0 eV to 15 eV, the N-2p, O-2p, and Sb-5p orbitals make the major contribution to both compounds. It is well known that the optical properties of compounds are mainly caused by electron transitions near the Fermi level. That is, the $[SbF_x]$ polyhedra and NO_3^- groups are primarily responsible for the linear and nonlinear optics of the title compounds. The results affirm the strategy that the synergistic effect of Sb^{3+} cations containing lone pair electrons and planar π-conjugated NO_3^- groups should be helpful in generating excellent optical properties, as confirmed by the electron density difference map. As shown in Fig. 3e and f, highly asymmetric lobes can be observed for the Sb^{3+} cations in $(NH_4)_3SbF_3(NO_3)_3$ and $(NH_4)_3SbF_4(NO_3)_2$, indicating the stereoscopic activity of lone pair electrons on Sb atoms. Meanwhile, a deepened N–O bond in the red electron cloud can be observed, indicating the presence of electron transfer in the π-conjugated NO_3^- unit.

Conclusions

Two antimony nitrates, $(NH_4)_3SbF_3(NO_3)_3$ and $(NH_4)_3SbF_4(NO_3)_2$, were successfully synthesized by adopting

low temperature molten salt synthesis. The discrepancy in stoichiometric ratios induces the diverse coordination environments of Sb^{3+}, which further results in the different macroscopic centricities of the two compounds. Owing to the synergistic effect of the π-conjugated NO_3^- group and the lone pair containing Sb^{3+} cations, both the compounds $(NH_4)_3SbF_3(NO_3)_3$ and $(NH_4)_3SbF_4(NO_3)_2$ reveal a large birefringence of 0.098@546 nm and 0.164@546 nm. NCS $(NH_4)_3SbF_3(NO_3)_3$ in particular has a strong SHG coefficient of about 3.3 × KDP, indicating that antimony nitrates are promising superior optical materials. The low temperature molten salt method provides a new way to overcome the difficulty in crystal growth which is easy hydrolysis and oxidation.

Conflicts of interest

There are no conflicts to declare.

Acknowledgements

The authors thank Dr Dingguo Xu at the College of Chemistry, Sichuan University, for help in the Vienna *Ab initio* Simulation Package calculations. This work was supported by the National Natural Science Foundation of China (no. 22122106, 22071158, 21971171).

References

1 H. P. Wu, B. B. Zhang, H. W. Yu, Z. G. Hu, J. Y. Wang, Y. C. Wu and P. S. Halasyamani, Designing Silicates as Deep-UV Nonlinear Optical (NLO) Materials using Edge-Sharing Tetrahedra, *Angew. Chem., Int. Ed.*, 2020, **59**, 8922–8926.

2 C. Wu, G. Yang, M. G. Humphrey and C. Zhang, Recent advances in ultraviolet and deep-ultraviolet second-order nonlinear optical crystals, *Coord. Chem. Rev.*, 2018, **375**, 459–488.

3 P. Yu, L. M. Wu, L. J. Zhou and L. Chen, Deep-ultraviolet nonlinear optical crystals: $Ba_3P_3O_{10}X$ (X = Cl, Br), *J. Am. Chem. Soc.*, 2014, **136**, 480–487.

4 L. Kang, F. Liang, X. X. Jiang, Z. S. Lin and C. T. Chen, First-Principles Design and Simulations Promote the Development of Nonlinear Optical Crystals, *Acc. Chem. Res.*, 2020, **53**, 209–217.

5 M. Mutailipu, Z. H. Yang and S. L. Pan, Toward the Enhancement of Critical Performance for Deep-Ultraviolet Frequency-Doubling Crystals Utilizing Covalent Tetrahedra, *Acc. Mater. Res.*, 2021, **2**, 282–291.

6 J. K. Zaręba, M. Nyk and M. Samoć, Nonlinear Optical Properties of Emerging Nano- and Microcrystalline Materials, *Adv. Opt. Mater.*, 2021, **9**, 2100216.

7 X. L. Chen and K. M. Ok, Metal oxyhalides: an emerging family of nonlinear optical materials, *Chem. Sci.*, 2022, **13**, 3942–3956.

8 X. H. Dong, L. Huang, H. M. Zeng, Z. E. Lin, K. M. Ok and G. H. Zou, High-Performance Sulfate Optical Materials Exhibiting Giant Second Harmonic Generation and Large Birefringence, *Angew. Chem., Int. Ed.*, 2022, **61**, e202116790.

9 W. F. Zhou, W. L. Liu and S. P. Guo, $(Na_{0.74}Ag_{1.26})BaSnS_4$: A New $AgGaS_2$-Type Nonlinear Optical Sulfide with a Wide Band Gap and High Laser Induced Damage Threshold, *Chem. – Eur. J.*, 2022, **28**, e202202063.

10 Z. H. Yang, C. Hu, M. Mutailipu, Y. Z. Sun, K. Wu, M. Zhang and S. L. Pan, Oxyhalides: prospecting ore for optical functional materials with large laser damage thresholds, *J. Mater. Chem. C*, 2018, **6**, 2435–2442.

11 J. Zhang, M. Abudoureheman, Z. Lian, J. W. Liu, Q. Wu and X. P. Xuan, Controllable Synthesis of Centrosymmetric/Noncentrosymmetric Phases for the Family of Halogen-Based Photonic Coordination Polymers to Enhance the Phase-Matching Second-Harmonic-Generation Response, *Inorg. Chem.*, 2022, **61**, 3716–3722.

12 X. Tian, Y. Xiao, B. Zhang, D. Yang and K. Wu, Novel structural transformation in K_3RePS_8 thiophosphates originating from the rare-earth (Re) cation sizes induced local coordination asymmetry, *Mater. Today Phys.*, 2022, **28**, 100885.

13 E. J. Cho, S. J. Oh, H. Jo, J. Lee, T. S. You and K. M. Ok, Layered Bismuth Oxyfluoride Nitrates Revealing Large Second-Harmonic Generation and Photocatalytic Properties, *Inorg. Chem.*, 2019, **58**, 2183–2190.

14 G. H. Zou and K. M. Ok, Novel ultraviolet (UV) nonlinear optical (NLO) materials discovered by chemical substitution-oriented design, *Chem. Sci.*, 2020, **11**, 5404–5409.

15 G. H. Zou, Z. E. Lin, H. M. Zeng, H. Jo, S. J. Lim, T. S. You and K. M. Ok, $Cs_3VO(O_2)_2CO_3$: an exceptionally thermostable carbonatoperoxovanadate with an extremely large second-harmonic generation response, *Chem. Sci.*, 2018, **9**, 8957–8961.

16 Y. X. Song, M. Luo, C. S. Lin and N. Ye, Structural Modulation of Nitrate Group with Cations to Affect SHG Responses in $RE(OH)_2NO_3$ (RE = La, Y, and Gd): New Polar Materials with Large NLO Effect after Adjusting pH Values of Reaction Systems, *Chem. Mater.*, 2017, **29**, 896–903.

17 Z. L. Chen, Z. J. Li, D. D. Chu, F. F. Zhang, X. J. Li, Z. H. Yang, X. F. Long and S. L. Pan, $A_2B_6O_9F_2$ (A = NH_4, K): new members of $A_2B_6O_9F_2$ family with deep-UV cutoff edges and moderate birefringence, *Chem. Commun.*, 2022, **58**, 12369–12372.

18 F. Yang, L. Wang, L. Huang and G. H. Zou, The study of structure evolvement of $KTiOPO_4$ family and their nonlinear optical properties, *Coord. Chem. Rev.*, 2020, **423**, 213491.

19 W. Zeng, X. H. Dong, Y. Tian, L. Huang, H. M. Zeng, Z. E. Lin and G. H. Zou, Unprecedented boat-shaped $[Mo_2O_5(IO_3)_4]^{2-}$ polyanions induced a strong second harmonic generation response, *Chem. Commun.*, 2022, **58**, 3350–3353.

20 G. Peng, C. S. Lin and N. Ye, $NaZnCO_3(OH)$: A High-Performance Carbonate Ultraviolet Nonlinear Optical

Crystal Derived from $KBe_2BO_3F_2$, *J. Am. Chem. Soc.*, 2020, **142**, 20542–20546.

21 L. Huang, Q. Wang, F. F. He, X. Y. Liu, Z. W. Chen, W. He, X. Y. Luo, D. J. Gao, J. Bi and G. H. Zou, Synthesis, crystal structures and nonlinear optical properties of polymorphism: α- and β-$RbHgI_3{\cdot}H_2O$, *J. Alloys Compd.*, 2019, **771**, 547–554.

22 B. L. Wu, C. L. Hu, F. F. Mao, R. L. Tang and J. G. Mao, Highly Polarizable Hg^{2+} Induced a Strong Second Harmonic Generation Signal and Large Birefringence in $LiHgPO_4$, *J. Am. Chem. Soc.*, 2019, **141**, 10188–10192.

23 G. Peng, Y. Yang, Y. H. Tang, M. Luo, T. Yan, Y. Q. Zhou, C. S. Lin, Z. S. Lin and N. Ye, Collaborative enhancement from Pb^{2+} and F^- in $Pb_2(NO_3)_2(H_2O)F_2$ generates the largest second harmonic generation effect among nitrates, *Chem. Commun.*, 2017, **53**, 9398–9401.

24 H. W. Yu, N. Z. Koocher, J. M. Rondinelli and P. S. Halasyamani, Pb_2BO_3I: A Borate Iodide with the Largest Second-Harmonic Generation (SHG) Response in the $KBe_2BO_3F_2$ (KBBF) Family of Nonlinear Optical (NLO) Materials, *Angew. Chem., Int. Ed.*, 2018, **57**, 6100–6103.

25 R. L. Tang, C. L. Hu, W. J. Xie, Q. M. Huang and J. G. Mao, $Bi_2[B_2(SeO_3)_6]$: A Metal Boroselenite with a Unique Zero-Dimensional $[B_2(SeO_3)_6]^{6-}$ Anionic Group and Large Birefringence, *Inorg. Chem.*, 2021, **60**, 3539–3542.

26 C. T. Chen, B. C. Wu, A. D. Jiang and G. M. You, A new-type ultraviolet SHG crystal β-BaB_2O_4, *Sci. Sin., Ser. B (Engl. Ed.)*, 1985, **28**, 235–243.

27 C. T. Chen, Y. C. Wu, A. D. Jiang, B. C. Wu, G. M. You, R. K. Li and S. J. Lin, New nonlinear-optical crystal: LiB_3O_5, *J. Opt. Soc. Am. B*, 1989, **6**, 616–621.

28 L. F. Mei, Y. B. Wang, C. T. Chen and B. C. Wu, Nonlinear optical materials based on $MBe_2BO_3F_2$ (M=Na,K), *J. Appl. Phys.*, 1993, **74**, 7014–7015.

29 S. G. Zhao, Y. Yang, Y. G. Shen, B. Q. Zhao, L. Li, C. M. Ji, Z. Y. Wu, D. Q. Yuan, Z. S. Lin, M. C. Hong and J. H. Luo, Cooperation of Three Chromophores Generates the Water-Resistant Nitrate Nonlinear Optical Material $Bi_3TeO_6OH(NO_3)_2$, *Angew. Chem., Int. Ed.*, 2017, **56**, 540–544.

30 X. H. Dong, L. Huang, Q. Y. Liu, H. M. Zeng, Z. E. Lin, D. G. Xu and G. H. Zou, Perfect balance harmony in $Ba_2NO_3(OH)_3$: a beryllium-free nitrate as a UV nonlinear optical material, *Chem. Commun.*, 2018, **54**, 5792–5795.

31 H. W. Yu, W. G. Zhang, J. Young, J. M. Rondinelli and P. S. Halasyamani, Bidenticity-Enhanced Second Harmonic Generation from Pb Chelation in $Pb_3Mg_3TeP_2O_{14}$, *J. Am. Chem. Soc.*, 2016, **138**, 88–91.

32 K. C. Chen, Y. Yang, G. Peng, S. D. Yang, T. Yan, H. X. Fan, Z. S. Lin and N. Ye, $A_2Bi_2(SO_4)_2Cl_4$ (A = NH_4, K, Rb): achieving a subtle balance of the large second harmonic generation effect and sufficient birefringence in sulfate nonlinear optical materials, *J. Mater. Chem. C*, 2019, **7**, 9900–9907.

33 J. L. Xie, Y. H. Zhou, L. H. Li, J. H. Zhang and J. L. Song, A new method for the preparation of a $[Sn_2(H_2PO_2)_3]Br$ SHG-active polar crystal via surfactant-induced strategy, *Dalton Trans.*, 2017, **46**, 9339–9343.

34 Y. L. Deng, L. Huang, X. H. Dong, L. Wang, K. M. Ok, H. M. Zeng, Z. E. Lin and G. H. Zou, $K_2Sb(P_2O_7)F$: Cairo Pentagonal Layer with Bifunctional Genes Reveal Optical Performance, *Angew. Chem., Int. Ed.*, 2020, **59**, 21151–21156.

35 M. C. Chen, L. M. Wu, H. Lin, L. J. Zhou and L. Chen, Disconnection Enhances the Second Harmonic Generation Response: Synthesis and Characterization of $Ba_{23}Ga_8Sb_2S_{38}$, *J. Am. Chem. Soc.*, 2012, **134**, 6058–6060.

36 H. J. Zhao, Y. F. Zhang and L. Chen, Strong Kleinman-Forbidden Second Harmonic Generation in Chiral Sulfide: La_4InSbS_9, *J. Am. Chem. Soc.*, 2012, **134**, 1993–1995.

37 M. Li, D. Zhou, C. P. Li and Z. Zhao, Low temperature molten salt synthesis of YAG: Ce spherical powder and its thermally stable luminescent properties after post-annealing treatment, *Mater. Sci. Semicond. Process.*, 2016, **44**, 101–107.

38 E. R. Cooper, C. D. Andrews, P. S. Wheatley, P. B. Webb, P. Wormald and R. E. Morris, Ionic liquids and eutectic mixtures as solvent and template in synthesis of zeolite analogues, *Nature*, 2004, **430**, 1012–1016.

39 X. H. Dong, L. Huang, C. F. Hu, H. M. Zeng, Z. E. Lin, X. Wang, K. M. Ok and G. H. Zou, $CsSbF_2SO_4$: An Excellent Ultraviolet Nonlinear Optical Sulfate with a $KTiOPO_4$ (KTP)-type Structure, *Angew. Chem., Int. Ed.*, 2019, **58**, 6528–6534.

40 V. M. B. Nunes, C. S. Queirós, M. J. V. Lourenço, F. J. V. Santos and C. A. Nieto de Castro, Molten salts as engineering fluids – A review: Part I. Molten alkali nitrates, *Appl. Energy*, 2016, **183**, 603–611.

41 A. A. Udovenko, N. I. Sigula, L. M. Volkova and R. L. Davidovich, Crystal structure of ammonium trinitrato-trifluoroantimonate(III), *Koord. Khim.*, 1979, **5**, 1711–1715.

42 G. Sheldrick, A short history of SHELX, *Acta Crystallogr., Sect. A: Found. Crystallogr.*, 2008, **64**, 112–122.

43 A. Spek, Single-crystal structure validation with the program PLATON, *J. Appl. Crystallogr.*, 2003, **36**, 7–13.

44 S. K. Kurtz and T. T. Perry, A Powder Technique for the Evaluation of Nonlinear Optical Materials, *J. Appl. Phys.*, 1968, **39**, 3798–3813.

45 M. D. Segall, J. D. L. Philip, M. J. Probert, C. J. Pickard, P. J. Hasnip, S. J. Clark and M. C. Payne, First-principles simulation: ideas, illustrations and the CASTEP code, *J. Phys.: Condens. Matter*, 2002, **14**, 2717.

46 P. E. Blochl, Projector augmented-wave method, *Phys. Rev. B: Condens. Matter*, 1994, **50**, 17953–17979.

47 G. Kresse, *VASP, 5.3.5*; **https://cms.mpi.univie.ac.at/vasp/vasp/vasp.html**, 2014.

48 G. Kresse and J. Furthmuller, Efficient iterative schemes for ab initio total-energy calculations using a plane-wave basis set, *Phys. Rev. B: Condens. Matter*, 1996, **54**, 11169–11186.

49 G. Kresse and D. Joubert, From ultrasoft pseudopotentials to the projector augmented-wave method, *Phys. Rev. B: Condens. Matter*, 1999, **59**, 1758–1775.

50 J. P. Perdew, K. Burke and M. Ernzerhof, Generalized Gradient Approximation Made Simple, *Phys. Rev. Lett.*, 1996, **77**, 3865–3868.

51 F. F. He, Q. Wang, C. F. Hu, W. He, X. Y. Luo, L. Huang, D. J. Gao, J. Bi, X. Wang and G. H. Zou, Centrosymmetric $(NH_4)_2SbCl(SO_4)_2$ and Non-centrosymmetric $(NH_4)SbCl_2(SO_4)$: Synergistic Effect of Hydrogen-Bonding Interactions and Lone-Pair Cations on the Framework Structures and Macroscopic Centricities, *Cryst. Growth Des.*, 2018, **18**, 6239–6247.

52 L. Wang, H. M. Wang, D. Zhang, D. J. Gao, J. Bi, L. Huang and G. H. Zou, Centrosymmetric $RbSnF_2NO_3$ vs. noncentrosymmetric $Rb_2SbF_3(NO_3)_2$, *Inorg. Chem. Front.*, 2021, **8**, 3317–3324.

53 F. F. He, Y. W. Ge, X. Y. Zhao, J. He, L. Huang, D. J. Gao, J. Bi, X. Wang and G. H. Zou, Two-stage evolution from phosphate to sulfate of new KTP-type family members as UV nonlinear optical materials through chemical cosubstitution-oriented design, *Dalton Trans.*, 2020, **49**, 5276–5282.

54 Y. Yang, Y. Qiu, P. F. Gong, L. Kang, G. M. Song, X. M. Liu, J. L. Sun and Z. S. Lin, Lone-Pair Enhanced Birefringence in an Alkaline-Earth Metal Tin(II) Phosphate $BaSn_2(PO_4)_2$, *Chem. – Eur. J.*, 2019, **25**, 5648–5651.

55 J. Chen, C. L. Hu, F. F. Mao, J. H. Feng and J. G. Mao, A Facile Route to Nonlinear Optical Materials: Three-Site Aliovalent Substitution Involving One Cation and Two Anions, *Angew. Chem., Int. Ed.*, 2019, **58**, 2098–2102.